ELSEVIER

Tectonophysics 344 (2002) 157–174

TECTONOPHYSICS

www.elsevier.com/locate/tecto

Tectonic analysis of an oceanic transform fault zone based on fault-slip data and earthquake focal mechanisms: the Húsavík–Flatey Fault zone, Iceland

Sebastian Garcia*, Jacques Angelier, Françoise Bergerat, Catherine Homberg

Laboratoire de Tectonique, UMR 7072 CNRS, Université Pierre et Marie Curie, Boîte 129, T25-26, 4 place Jussieu, 75252 Paris Cedex 05, France

Received 4 May 2001; accepted 6 December 2001

Abstract

The Húsavík–Flatey Fault (HFF) is an oblique dextral transform fault, part of the Tjörnes Fracture Zone (TFZ), that connects the North Volcanic Zone of Iceland and the Kolbeinsey Ridge. We carry out stress inversion to reconstruct the paleostress fields and present-day stress fields along the Húsavík–Flatey Fault, analysing 2700 brittle tectonic data measured on the field and about 700 earthquake focal mechanisms calculated by the Icelandic Meteorological Office. This allows us to discuss the Latest Cenozoic finite deformations (from the tectonic data) as well as the present-day deformations (from the earthquake mechanisms). In both these cases, different tectonic groups are reconstructed and each of them includes several distinct stress states characterised by normal or strike-slip faulting. The stress states of a same tectonic group are related through stress permutations ($\sigma_1-\sigma_2$ and $\sigma_2-\sigma_3$ permutations as well as $\sigma_1-\sigma_3$ reversals). They do not reflect separate tectonic episodes. The tectonic groups derived from the geological data and the earthquake data have striking similarity and are considered to be related. The obliquity of the Húsavík–Flatey Fault implies geometric accommodation in the transform zone, resulting mainly from a dextral transtension along an ENE–WSW trend. This overall mechanism is subject to slip partitioning into two stress states: a Húsavík–Flatey Fault-perpendicular, NE–SW trending extension and a Húsavík–Flatey Fault-parallel, NW–SE trending extension. These three regimes occur in various local tectonic successions and not as a regional definite succession of tectonic events. The largest magnitude earthquakes reveal a regional stress field tightly related to the transform motion, whereas the lowest magnitude earthquakes depend on the local stress fields. The field data also reveal an early extension trending similar to the spreading vector. The focal mechanism data do not reflect this extension, which occurred earlier in the evolution of the HFF and is interpreted as a stage of structural development dominated by the rifting process.

Keywords: Iceland; transform zone; stress regimes; focal mechanism; strike-slip and normal faults; transtension; Slip partitioning

1. Introduction

The Tjörnes Fracture Zone (TFZ) is an oceanic transform zone (Ward, 1971; Saemundsson, 1974) connecting the Kolbeinsey Ridge, part of the Mid-Atlantic Ridge, with the North Volcanic Zone of Iceland (Fig. 1). The Húsavík–Flatey Fault (HFF) is

* Corresponding author. Fax: +33-1-44-27-50-85.
E-mail address: sebastian.garcia@lgs.jussieu.fr (S. Garcia).

0040-1951/02/$ - see front matter
PII: S0040-1951(01)00282-7

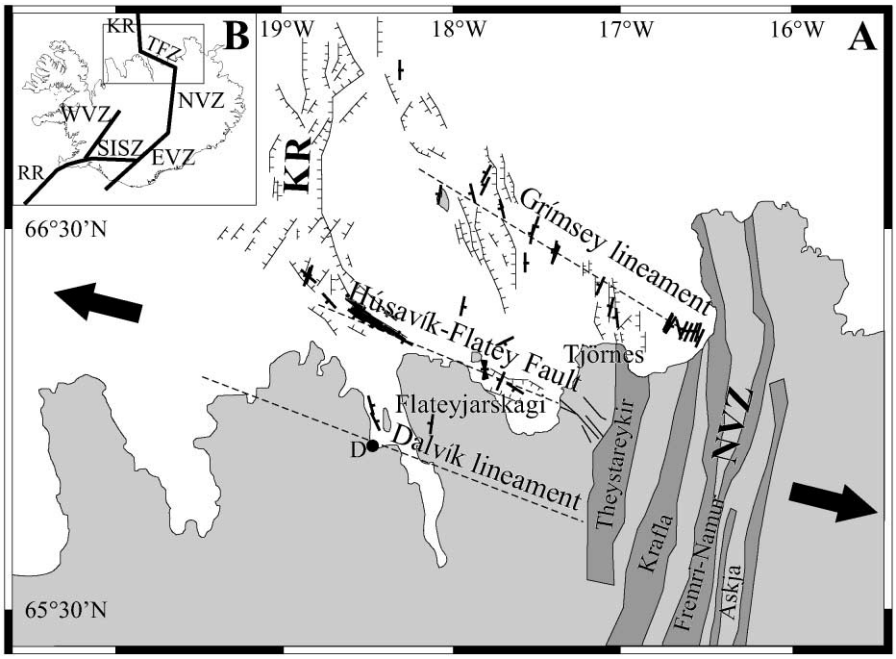

Fig. 1. The Tjörnes Fracture Zone. (A) Dashed lines indicate the three major structures of the Tjörnes Fracture Zone. Black thin lines: offshore (with barbs) and onshore (without barbs) faults mapped with conventional reflection seismic methods or by direct observations on land. Black thick lines: fault segments inferred from accurate relative locations of microearthquakes (after Rögnvaldsson et al., 1998). Black arrows indicate the direction of plate motion (DeMets et al., 1990, 1994). Land areas are shaded. The four main fissure swarms of the North Volcanic Zone (NVZ) are indicated in dark grey. KR: Kolbeinsey Ridge, D: Dalvík. (B) Inset: rift zone segments and transform faults in Iceland (EVZ: East Volcanic Zone, WVZ: West Volcanic Zone, SISZ: South Iceland Seismic Zone, TFZ: Tjörnes Fracture Zone, RR: Reykjanes Ridge).

one of the main active structures of the TFZ (Einarsson and Björnsson, 1979). The HFF is of special geological interest because part of it is exposed on land, on the Tjörnes Peninsula and at the northern extremity of the Flateyjarskagi Peninsula (Fig. 1A). It can therefore be studied in detail in the field.

Despite the general agreement on the significance of the HFF as a right lateral rift–rift transform fault, the interpretation of its geological structures and hence its tectonic evolution are controversial, as discussed by Bergerat et al. (2000). The choice between the proposed interpretations depends on the constraints available in terms of tectonic regimes. Detailed investigations have been carried out for dykes, major faults and mineral veins (Young et al., 1985; Fjäder et al., 1994), but the potential for reconstructing tectonic regimes based on microtectonic considerations has not been fully exploited. Such a systematic field study had been undertaken since 1997 (Bergerat et al., 2000; Angelier et al., 2000).

In the present paper, we aim at elucidating the tectonic evolution of the HFF, based on detailed observations and analysis of brittle structures on the Flateyjarskagi Peninsula (Fig. 1A) combined with earthquake focal mechanisms analysis. The brittle tectonic data mainly constrain the Latest Cenozoic finite deformation whereas the seismological data constrain the present-day deformation. Studying tectonics at these different time scales allows a better understanding of the behaviour of the HFF. In particular, we aim to settle if its evolution corresponds to a succession of several distinct regimes or to relatively minor variations within a single overall regime.

2. Geological and structural setting

The TFZ (Fig. 1) is a WNW–ESE trending oceanic transform zone with a dextral component (Ward, 1971; Saemundsson, 1974) and is active since 7–9

Ma. Its development can be interpreted as a consequence of an eastward shift of the rift zone in Iceland, from its previous location in western Iceland to its present location (e.g., Ward, 1971; Saemundsson, 1974; Helgason, 1984, 1985).

The TFZ is seismically active (Fig. 2). Instrumentally recorded earthquakes reach magnitude 7 (Einarsson and Björnsson, 1979). The seismic zone is about 120 km long and 70 km wide, but most of the seismic activity is confined to three major active structures: the Grímsey lineament, the Húsavík–Flatey Fault and the Dalvík lineament, from north to south (Einarsson and Björnsson, 1979).

The Grímsey lineament has no clear tectonic evidence onshore. It can only be traced offshore based on the seismicity (Fig. 2), and trends N128°E on average (Rögnvaldsson et al., 1998). It not seems to be a continuous fault but rather composed of "en échelon" structures. Indeed, most of the offshore active faults (Fig. 1A) are NNW–SSE trending normal faults and N–S trending left-lateral strike-slip faults with significant dip–slip component (Rögnvaldsson et al., 1998).

The Húsavík–Flatey Fault (HFF) is the only fault zone with a clear onshore expression. It can be followed on the Tjörnes Peninsula (Saemundsson, 1974), where it trends N115°E on average (Fjäder et al., 1994) over a distance of about 25 km until its merges in the N–S trending Theystareykir fissure swarm (Fig. 1A). The HFF offsets the geological units by at least 5–10 km to a maximum of 60 km (Saemundsson, 1974). On the Tjörnes Peninsula, the Tertiary pre-Pliocene basalts crop out in tectonic contact across the HFF with the basalts of upper Matuyama age (i.e., Plio–Pleistocene). The age difference between the rocks on both sides of the fault thus reaches at least 5 Ma (Saemundsson, 1974). Offshore, Rögnvaldsson et al. (1998) have identified dextral movements along seismic faults striking between N113°E and N146°E (Fig. 1A). East of the Flatey Island (see Fig. 3 for location), these dextral movements coexist with left-lateral strike-slip on NNE–SSW faults (Fig. 1A). NW–SE trending normal faults are also present (McMaster et al., 1977). Onshore, this NE–SW extension has been evidenced by transform-parallel dyke swarms and numerous minor normal faults (Gudmundsson et al., 1993; Fjäder et al., 1994; Gudmundsson and Fjäder, 1995; Langbacka and Gudmundsson, 1995; Angelier et al., 2000; Bergerat et al., 2000). On the Tjörnes Peninsula, the vertical displacement across the HFF can reach 1400 m (Tryggvason, 1973). On the Flateyjarskagi Peninsula, the main structures described above (WNW–ESE normal faults, WNW–ESE right-lateral strike-slip faults and NNE–SSW left-lateral strike-slip faults) are also present (Young et al., 1985; Fjäder et al., 1994; Gudmundsson and Fjäder, 1995; Jancin et al., 1995; Angelier et al., 2000; Bergerat et al., 2000). It is considered that the Krafla rifting event (1975–1984) locked the HFF since early 1976. However, renewed seismicity on the HFF in 1994 at its western extremity and small seismic activity in 1997 along its eastern part may indicate that the HFF is currently being unlocked. The releasing should migrate along the fault from Northwest to Southeast (Rögnvaldsson et al., 1998; Gudmundsson, 2000).

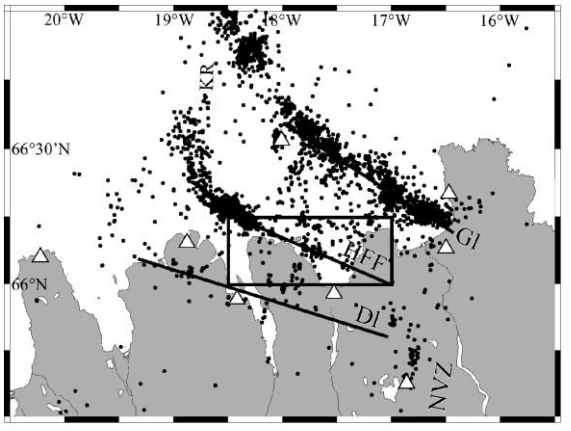

Fig. 2. Seismic map of the Tjörnes Fracture Zone for the period 1995–1997. The Dalvík lineament (Dl), the Húsavík–Flatey Fault (HFF) and the Grímsey lineament (Gl) are underlined by black lines. Earthquakes of magnitude superior or equal to 1 are represented as black dots. The rectangle includes earthquakes used in this paper. White triangle: seismometers of the SIL network.

The WNW–ESE Dalvík lineament is seismically identified, although its present seismic activity is pretty poor (Fig. 2). Despite its onshore morphological expression along the Dalsmynni valley on the Flateyjarskagi Peninsula (Fig. 3), there is little or no structural evidence for a large WNW–ESE strike-slip fault zone in this area. Movements probably take place along N–S trending left-lateral strike-slip faults (Fig. 1A), as defined by Rögnvaldsson et al. (1998) near the Dalvík lineament. Similar N–S trending

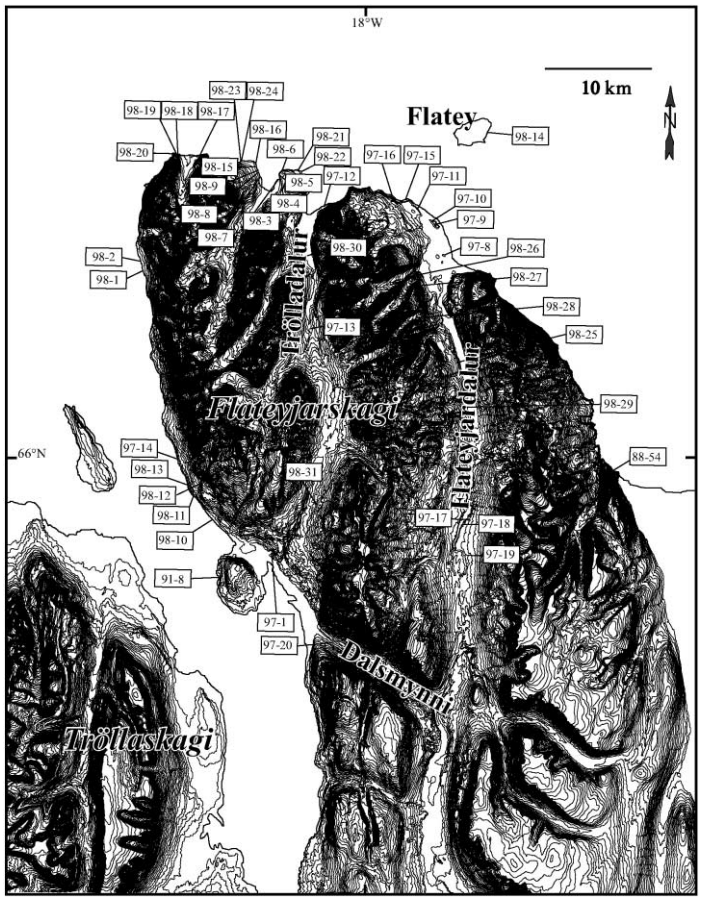

Fig. 3. Morphological feature of the Flateyjarskagi Peninsula and location of the sites of measurements. See Fig. 1 for location of the peninsula. Main valleys (corresponding to major faults or major joint systems) are indicated.

ruptures have been mapped after the *M*6.2 earthquake that occurred in 1934 near the Dalvík city (Fig. 1A) (Thorarinsson, 1937, referred to in Langbacka and Gudmundsson, 1995).

Because the Húsavík–Flatey Fault and the Dalvík and Grímsey lineaments form an angle of about 60° with the average trend of the rift zones (striking N000°–N010°E), the TFZ clearly belongs to the oblique transform type.

3. Paleostresses and brittle deformation along the Húsavík–Flatey Fault

A detailed analysis of the brittle structures along the HFF, with particular emphasis on the tectonic features relevant for determining the paleostress orientations is presented. The total data set considered herein contains 2700 data, including approximately 2100 fault slip data, 500 extension fractures (dykes and mineral veins) and 100 bedding planes. They were collected on the Flateyjarskagi Peninsula (Fig. 3); 1200 data during the field campaigns of 1988, 1991 and 1997 (Angelier et al., 2000; Bergerat et al., 2000) and 1500 new data in 1998. Most of the 47 sites where we collected the data are tholeiitic lava piles, which range in age between approximately 9.5 and 12.5 Ma according to Jancin et al. (1985). To determine the sense of slip on striated fault planes, we used a variety of criteria (Angelier, 1994) such as mineralised steps, polished vs. rough surfaces, Riedel fractures, etc. All observable relative chronology rela-

tionships between the brittle structures have been recorded, as well as those inferred from the geometrical relationships between the brittle systems and the tilt of the lava pile.

3.1. Distribution of brittle structures

The fault population consists of strike-slip, normal and some reverse faults. For each of these three types, a selection was made considering the dip of the fault plane and the pitch of the striae. Although the criteria shown in Table 1 are partly arbitrary, they aim at minimising the bias introduced by the presence of tilted fault patterns. Such biases are illustrated by systems of conjugate normal faults that developed before (or during) block tilting: some faults appear to be reverse in the present-day, post-tilt configuration, whereas other faults remain normal. For this reason, we introduced some bounds in the geometrical selection. For instance, a reverse fault that dips 45° or steeper is not incorporated in the reverse fault set. Consequently, the total data set used in this analysis (i.e., 2000 fault slip data) is not as large as the original data set (i.e., 2100 fault slip data). Because the sense of strike-slip motion is critical in paleostress studies, left-lateral and right-lateral senses have been distinguished in Table 1. Furthermore, other brittle data such as extension fractures (dykes and minerals veins), because of their interest in terms of stress reconstruction, are considered in Table 1.

Based on this separation, a preliminary study of the tectonic features can be performed. The strike-slip faults (Table 1) represent the largest group (44%, 1105 data). Inside this group, the numbers of left-lateral and of right-lateral motions differ slightly and represent 25.3% (635 data) and 18.7% (470 data) of the total data set, respectively (Table 1). The second largest group is the normal fault group (almost 34%, 846 data), whereas the reverse fault group is very small (about 1%, 32 data). Because all faults were systematically measured, these percentages are significant in terms of fault frequency in the studied area. In addition, 21% of our data (528 data) correspond to extension structures (dykes and mineral veins). This proportion does not reflect the actual one because the vein measurements were not systematically collected in the outcrops. That Gudmundsson et al. (2001) could measure more than 1700 mineral veins in a limited number of sites on the same peninsula shows that tension veins are extremely common.

Table 1
Classification and percentage of brittle structures

	Dip		Pitch		%	
	Min.	Max.	Min.	Max.		
Strike-slip faults	75	90	0	45	44	R: 18.7 L: 25.3
Normal faults	45	75	45	90	33.7	
Reverse faults	15	45	45	90	1.3	
Extension fractures					21	

R: Right-lateral strike-slip faults, L: Left-lateral strike-slip faults. Extension fractures are mineralised veins and dykes (shaded cell). See detailed explanation in text for the classification.

The 2000 selected fault slip data and all the extension fractures were represented in separate rose diagrams (Fig. 4). A variety of fault and fracture strikes exist (Fig. 4a–e). The predominant direction for the normal faults, the extension fractures and the left-lateral strike-slip faults is NNE–SSW to NE–SW (Fig. 4a, b and e, respectively) and also NW–SE to NNW–SSE for the normal faults (Fig. 4a) and for the right-lateral strike-slip faults (Fig. 4d). These directions fit well the large-scale structures, especially the normal and strike-slip faults, described in the literature by Young et al. (1985) and Fjäder et al. (1994). Therefore, the small-scale tectonic features can be considered representative in terms of brittle deformation.

In addition to the brittle tectonic data, the poles of the measured bedding planes are shown in stereoplot (Fig. 4f). Significant tilting has occurred in the studied region, in relation to faulting. Indeed, Young et al. (1985) and Fjäder et al. (1994) have observed that the dip direction of the lava pile changes from 30° to 45° to the NW on the northern coast to 10–15° to the SW in the centre of the peninsula. The orientations inferred from our data are consistent with these observations, even if the site distribution (Fig. 3) certainly introduces a statistical bias. For instance, because the sites and the measurements were more numerous in the northern part of the peninsula, the northern dip direction of the lava pile (30–45° to the NW) is better represented in our diagrams than the southern lava dip of 10–15° to the SW.

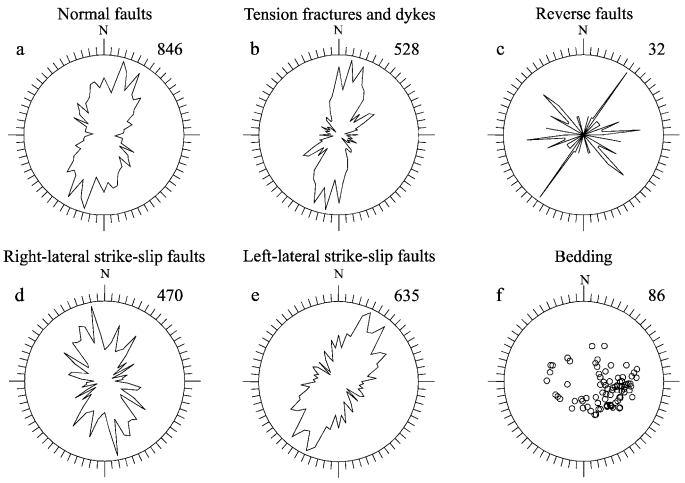

Fig. 4. Measured structural elements. Rose diagrams for strikes of normal faults (a), extension fractures and dykes (b), reverse faults (c), right-lateral strike-slip faults (d), left-lateral strike-slip faults (e) and poles to bedding (f). Number of data is indicated for each kind of tectonic feature.

3.2. From minor faults to local stress states

Paleostresses associated with the minor faults were determined using the direct inversion method (Angelier, 1990). Following this method, it is aimed at finding the best possible fit between the measured and calculated fault slip through the search of a common stress tensor. One thus obtains the orientation of the three principal stress axes σ_1, σ_2 and σ_3, with $\sigma_1 \geq \sigma_2 \geq \sigma_3$ (pressure being considered positive) and the Φ ratio between the principal stress differences $[\Phi=(\sigma_2-\sigma_3)/(\sigma_1-\sigma_3)]$, with $0 \leq \Phi \leq 1$. The dykes and extension fractures are taken into additional account and are interpreted as mode I fractures, the minimum principal stress direction σ_3 is considered as perpendicular to their trends.

In the Anderson model (Anderson, 1942), one of the principal stress axes is assumed to be vertical, so that the other two axes are horizontal. The determination of stress tensors adopted herein does not include such an assumption. Where the calculated tensor did not display nearly vertical and horizontal attitudes of the three principal stress axes, the relation to the attitude of the tilted lava flows provided good indication that the corresponding fault set had been tilted with the bedding after its formation. In such cases, one of the stress axes was often found to be perpendicular to bedding, whereas the two others were lying within the bedding plane. A simple back-tilting process restored the horizontal and vertical attitudes of the principal stress axes (exceptions exist, with a necessary back-tilt angle smaller than the dip angle of the tilted lava flows, and generally result from syn-tilting faulting).

Fig. 5a illustrates the stress inversion result for a monophase site (site 98-11, see location in Fig. 3). For this site, no separation of the data was necessary to obtain the best fit between the fault slips and the calculated stress tensor (revealing computed N086°E trending extension). In contrast, in areas where complex deformation has occurred, the brittle deformation at a given site commonly involves two or more tectonic regimes. The collected data at the site 98-26 (Fig. 5b, see location in Fig. 3) show unacceptably mechanical incompatibility when determining a single stress tensor, suggesting a polyphase deformation. The tensor determinations that could be considered acceptable involved calculation of four stress states that correspond to an extension regime with computed σ_3 trending N112°E and three strike-slip regimes with computed σ_3 trending N274°E, N359°E and N321°E.

A weight, ranging from 1 to 4 (from lowest to highest quality), is attributed to each tensor, in order to express its accuracy (the higher accuracy, the largest weight). Regarding the data, this accuracy increases with the number of data, their azimuthal dispersion and the existence of conjugate fault pattern. Regarding the inversion process, the accuracy decreases when the average misfit between the calculated shear stress and

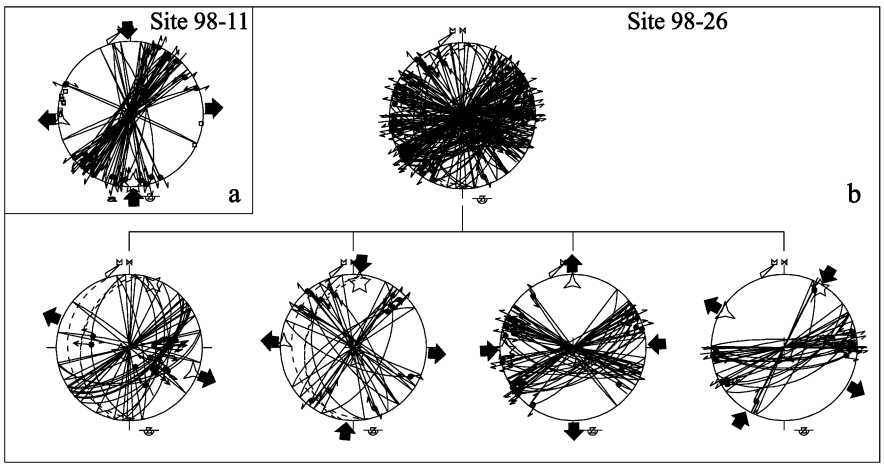

Fig. 5. Example of monophase (a) and polyphase (b) measurement sites. The polyphase site needs a separation of data in four subsets. Diagrams in lower hemisphere and equal area projection. Faults as thin lines, bedding as dashed lines, poles to extension fractures as circles and slickenside lineations as dots with single (centrifugal-normal) or double (left- or right lateral) arrows. Maximum (σ_1), intermediate (σ_2) and minimal (σ_3) stresses as three-, four- and five-branched stars, respectively. Direction of extension or compression as large black arrows. N: geographic North, M: magnetic North. See Fig. 3 for location of the sites 98-11 and 98-26.

the slip vector becomes large. For example, a weight factor 4 was attributed to the tensor at site 98-11 (Fig. 5a), whereas a weight factor 2 was given to the normal-type tensor at site 98-26 (Fig. 5b).

3.3. Inversion results

Using the direct inversion method, a total of 159 stress tensors were determined for 47 localities: 90 appeared to be of strike-slip type (i.e., with σ_2 close to vertical) and 69 of normal type (i.e., with σ_1 close to vertical). Most reverse faults appeared to be tilted normal faults. A single stress tensor of genuine reverse type (i.e., with σ_3 close to vertical) could be determined. Furthermore, because of its Φ ratio close to zero (indicating nearly similar magnitudes for σ_2 and σ_3), and considering the similarity in σ_1 trends with respect to other determinations, it will be included in the strike-slip tensor family. Considering the whole data set (i.e., 2700 brittle data), 18% of it were discarded during the inversion process because it was impossible to include them in a mechanically homogeneous set without reaching high misfit level.

For both the normal and strike-slip tensors, six subsets have been determined by grouping tensors that have similar σ_3 trends. An average σ_3 trend has been calculated for each of the 12 subsets (six normal subsets and six strike-slip subsets), taking into account the weight ranging attributed at each tensor (Table 2). The six strike-slip states of stress, named S1, S2, S3, S4, S5 and S6 (with an uppercase S indicating strike-slip regime and an arbitrary index), have a mean σ_3 trending N101±7°E, N081±5°E, N057±6°E, N134±9°E, N168±8°E and N022±7°E, respectively (Table 2 and Fig. 6). The six normal states of stress have a mean σ_3 striking N107±7°E, N078±6°E, N046±9°E, N129±6°E, N161±8°E and N019±5°E. As each of normal states of stress shows a similar direction of extension to one of the strike-slip states of stress, they have been labelled N1, N2, N3, N4, N5 and N6, respectively, in order to underline this similarity (Table 2 and Fig. 6).

To explain the geometrical relationships between some of these stress states, a simple stress permutation, or switch, between σ_1 and σ_2, can be invoked. Such an interchange is a common phenomenon in extensional tectonics (Angelier and Bergerat, 1983). We can consequently group pairwise strike-slip states of stress and normal states of stress according to similarities in σ_3 trends, and thus define six main tectonic regimes (Table 2 and Fig. 6). They correspond to extensions that trend WNW–ESE (S1–N1), ENE–WSW (S2–N2), NE–SW (S3–N3), NW–SE (S4–N4), NNW–SSE (S5–N5) and NNE–SSW (S6–N6).

Table 2
Directions of minimal principal stress inferred from fault slip inversion

Site	Stress state											
	S1	N1	S2	N2	S3	N3	S4	N4	S5	N5	S6	N6
88-54		100*3										
91-8	98*4											14*3
97-1			79*3					129*1			35*2	
97-8	111*4					47*1			179*3		27*2	
97-9	99*2						146*4			153*2	9*3	21*1
97-10			83*4			35*4	135*1	128*4			27*3	
97-11	100*3	115*3					145*3		172*3			
97-12	98*3		80*2		44*2	61*4	126*1	130*1				
97-13	96*4							123*2			15*2	
97-14		113*2	80*4									
97-15	94*3	101*4					138*4		173*2		29*2	
97-16		117*3	71*2					133*1	162*2			
97-17			87*1			38*3			171*1		15*1	
97-18	103*2			87*2		43*1				160*2		
97-19			74*3				121*1	141*1	163*2			
97-20	92*4								165*2		22*3	17*1
98-1		104*2	80*4									
98-2	114*2		81*1						171*3			
98-3	114*2		79*2			48*3	123*2	138*1				
98-4		100*1	88*3	71*1								
98-5	98*3											
98-6						54*3	123*3					
98-7						62*1			156*3		10*3	
98-8	98*4			87*1						153*2		
98-9			73*3	82*3								
98-10					58*2						28*1	
98-11			86*4									
98-12							125*1					
98-13											24*4	
98-14						40*4						
98-15		103*4				55*1			161*4			22*1
98-16		97*1						123*3	160*3		18*2	
98-17				72*4			129*1				18*1	
98-18	94*4					64*1		133*1		171*2	23*1	
98-19			81*4	87*1				124*1				
98-20	116*4				60*2	42*4		125*1				
98-21		111*1	87*3					123*1	176*2			25*2
98-22	110*3	102*4			62*4	50*4				176*1		
98-23	100*2	110*4				36*2					31*1	
98-24		106*3	84*4						157*1			
98-25				69*1		39*2	129*4	123*1			15*2	
98-26	94*4	112*2		73*2		43*1	141*3		179*4			
98-27	102*4	98*1			56*3				161*2		26*1	
98-28	102*3	119*3	78*4	80*1		37*2					17*4	
98-29						55*3	130*3	140*3			32*2	
98-30				74*1								
98-31									170*3	159*1		
Extrema	92/116	97/119	71/88	69/87	44/62	35/64	121/146	123/141	156/179	153/176	9/35	14/25
σ_3 Azimuth	101±7	107±7	81±5	78±6	57±6	46±9	134±9	129±6	168±8	161±8	22±7	19±5

Table 2 (*continued*)

Site	Stress state											
	S1	N1	S2	N2	S3	N3	S4	N4	S5	N5	S6	N6
Number of sites	20	16	17	10	5	18	13	14	16	6	19	5
	36		27		23		27		22		24	
Data %	18.2	9.6	11.9	6.7	2.5	12.3	8	6.7	8.8	3.4	9.3	2.5
	27.8		18.6		14.8		14.7		12.2		11.8	
Weight %	17	11	12	4	3	11	8	6	13	3	10	2
	28		16		14		14		16		12	

For each stress state, trends of minimal horizontal stress (σ_3) is indicated (S: strike-slip type, N: normal type) as well as a weighting criteria, varying from 1 to 4. See text for further explanations. The main and extreme values of σ_3 are indicated, considering the weighting criteria at the bottom of the table. The number of sites where each stress state had been found (we collected data in 47 sites), the percentage of measured data corresponding to each one (we used more than 2100 data) and the weight percentage of the tensors are also indicated. For the three bottom lines, the upper cells refer to the two stress states of each tectonic regime (S and N), whereas the lower cell refers to the tectonic regime taken as a whole.

To evaluate the relative importance of these six tectonic regimes, we considered for each pair of stress states (1) the number of sites where they have been identified, (2) the percentage of associated faults (relative to the total set), and (3) the weight percentage of the corresponding tensors (Table 2). According to this analysis, the S1–N1 regime (WNW–ESE extension) is the most important tectonic regime that has affected the Flateyjarskagi Peninsula. It was identified in a majority of sites and represents 27.8% of the data. The second tectonic regime is the S2–N2 regime (ENE–WSW extension), which represents 18.6% of the data (Table 2). The remaining regimes contain less data and are almost equally represented. Indeed, S3–N3, S4–N4, S5–N5 and S6–N6 are effectively found in comparable number of sites (23, 27, 22 and 24 sites, respectively), and correspond to similar percentages of the total data set (14.8%, 14.7%, 12.2% and 11.8%, respectively).

3.4. Chronological relations between the main tectonic regimes

The chronological criteria are based on the observation of superposed fault striae on reactivated fault planes, crosscutting of faults or dykes and geometrical relationships with block tilting. These criteria were searched for and carefully examined in order to establish the chronological order of the six main tectonic regimes. In spite of determining 51 relative chronology data it was difficult to reconstruct a clear and complete chronology.

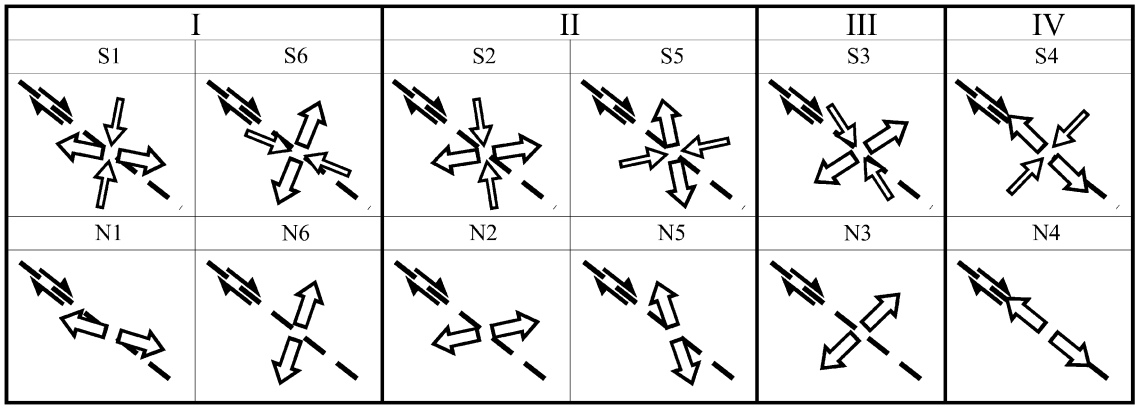

Fig. 6. Paleostress states inferred from brittle data (N, S: normal and strike-slip stress states, respectively). The empty arrows indicate the direction of compression and extension. The trend of the HFF (dashed line) and its strike-slip movement are indicated. North on the upward direction. See text for detailed explanations concerning the grouping in four tectonic groups.

Numerous relative chronology data clearly suggest that the S1–N1 regime (the WNW–ESE extension) is the oldest one. The second and third regimes in the succession could be the S4–N4 regime (NW–SE extension) and the S3–N3 regime (NE–SW extension), but their chronological order is not clear. The fourth regime could be the S6–N6 regime (NNE–SSW extension), probably followed by the S5–N5 regime (NNW–SSE extension). The S2–N2 regime (ENE–WSW extension) may have taken place at any time after the S4–N4 and the S3–N3 regimes. These apparent discrepancies suggest that intricate succession of regimes have taken place in time.

3.5. Spatial variation of the brittle deformation

Young et al. (1985) and Fjäder et al. (1994) pointed out that the brittle deformation increases close to the HFF. For Fjäder et al. (1994), intense deformation is restricted to a 3- to 5-km-wide zone along the north coast of the peninsula. In contrast, for Young et al. (1985), high deformation marked by block rotations due to a heterogeneous simple shear was found in an 11-km-wide shear zone bounded to the north by the HFF.

The density of brittle structures on the Flateyjarskagi Peninsula obviously decreases from north to south. However, any attempt at defining accurate quantitative estimates of the density of fracturing and faulting through the peninsula is biased by the inhomogeneous distribution of the data collection sites (Fig. 3). Furthermore, in the southern part of the studied area, an additional difficulty emerges, as a result of the superimposition of deformations respectively induced by the Dalvík lineament and by the HFF.

3.6. Mechanical interpretation

Strike-slip states of stress are dominant for the S1–N1, S2–N2, S5–N5 and S6–N6 regimes (Table 2). Furthermore, the S5 and S6 stress states exhibit directions of extension (σ_3 trends) nearly perpendicular to those of S2 and S1, respectively (Fig. 6). We concluded that this near-perpendicular relationship is a consequence of a drastic permutation of σ_1 and σ_3. A variety of phenomena such as elastic stress relaxation (Du and Aydin, 1996), elastic rebound, dyke injections, tilted block accommodations or abrupt stress drops may be invoked in order to account for such permutations. As an illustration of a permutation of σ_1 and σ_3, a rift-parallel contraction of the surface in areas adjacent to the active rifting zone has been noticed by several authors (e.g., Björnsson et al., 1979; Möller and Ritter, 1980; Wendt et al., 1985; Foulger et al., 1992) during the last Krafla rifting event (1975–1984).

The same reasoning can, however, hardly be applied to regimes S3–N3 and S4–N4 (Fig. 6) because the normal state of stress of these regimes clearly prevails (S3–N3, see Table 2), or is similar in importance, as compared with the strike-slip state of stress. Nevertheless, these stress regimes are particular with respect to the regional transform trend, because the stress axes are parallel or perpendicular to the transform fault (Fig. 6).

As indicated in Fig. 6, our results can be reduced in terms of four tectonic groups: I, II, III and IV, respectively. Two of these groups are composed of two tectonic regimes characterised by a switch between the σ_1 and σ_3 axes for the strike slip modes. The major extensional trend is WNW–ESE for S1–N1 (coupled with the S6–N6 opposite regime, compare S1 and S6), ENE–WSW for S2–N2 (coupled with the S5–N5 opposite regime, compare S2 and S5), NE–SW for S3–N3, and NW–SE for S4–N4. However, these regroupings do not fit well with the tectonic regime succession determined by chronological relationships. This problem will be considered in the discussion.

4. Seismicity and present-day stresses along the Húsavík–Flatey Fault

The Tjörnes Fracture Zone is an area of intense seismic activity (Fig. 2). Because of the existence of the local network operated by the Icelandic Meteorological Office, numerous double couple focal mechanisms of earthquakes are available and allow reconstruction of the stresses that govern the present-day activity of the TFZ.

4.1. The data

The SIL network of the Icelandic Meteorological Office is composed of 37 stations mainly distributed in south part of Iceland. Each station is equipped with

Table 3
Relative percentages of the different regimes of focal mechanisms of earthquakes (SSR: strike-slip regime, NR: normal regime, RR: reverse regime) and subsets of regimes considered in the studied area

Regime	Subset	% of data		% of data by regime	
SSR	2	70.3	31.4	100	44.7
	3		33.2		47.2
	4		3		4.3
	5		2.7		3.8
NR	2	18.4	5.4	100	29.3
	3		8.2		44.7
	4		4.8		26
RR	3	11.3	1.8	100	15.8
	4		9.5		84.2

See the text for explanations about separation. Two statistic analyses had been made. In the first case, we considered all the regimes or subsets of regimes (the summation of the three regimes or of the nine subsets equals 100%) whereas in the second, we considered each regime independently (the summation for each regime equals 100%). See Fig. 9 for orientations of stress axes.

three-component seismometers. The network functioning is highly automatic and allows routine analysis of the seismic recordings (Stefansson et al., 1993; Bödvarsson et al., 1996). The double couple mechanism is obtained using the source mechanism inversion method developed by Slunga (1981) and extended by Rögnvaldsson and Slunga (1993). The maximum error on strike, dip and rake of the nodal planes is 15° for earthquakes with local magnitude (M_L) smaller than 0.5 (Rögnvaldsson and Slunga, 1993).

Six seismological stations were installed in northern Iceland in December 1993, and three additional stations were installed in 1996. Stations are separated from each other by about 40–60 km (Fig. 2). Thus, with respect to the density of the network, the detection threshold is fixed at M_L 0.5 (Stefansson et al., 1993; Bödvarsson et al., 1996). Because most of the seismicity occurs in the offshore parts of the TFZ, the theoretical uncertainty in the routinely determined hypocenter locations varies from 2 to 10 km.

In this study, we considered the seismic events recorded by the SIL network along the HFF (Fig. 2) from 1995 to 1997. Out of a total of nearly 4000 earthquakes, we used the 669 events with a magnitude larger than M_L 1, in order to discard poorly constrained mechanisms. The largest local magnitude in this data set is 4.8. This earthquake was located in the NW corner of the rectangle in Fig. 2.

4.2. Geometrical separation of focal mechanisms

The data reveal that the present-day seismicity includes focal mechanisms with nearly vertical P, B or T axes, corresponding to strike-slip mechanisms (70.3% of the total set), normal mechanisms (18.4%) and reverse mechanisms (11.3%), respectively (Table 3). Although these axes should not be viewed as mechanical axes, they bisect the pressure and tension quadrants that have mechanical significance (McKenzie, 1969; Angelier and Mechler, 1977). The strike-slip, normal and inverse mechanisms thus reflect variations in the stress regime and need to be considered separately.

Inside a mechanical group (such as the strike-slip mechanisms), many pairs of earthquake mechanisms exhibit incompatible extensional and contractional quadrants (see Fig. 7). This indicates that more than

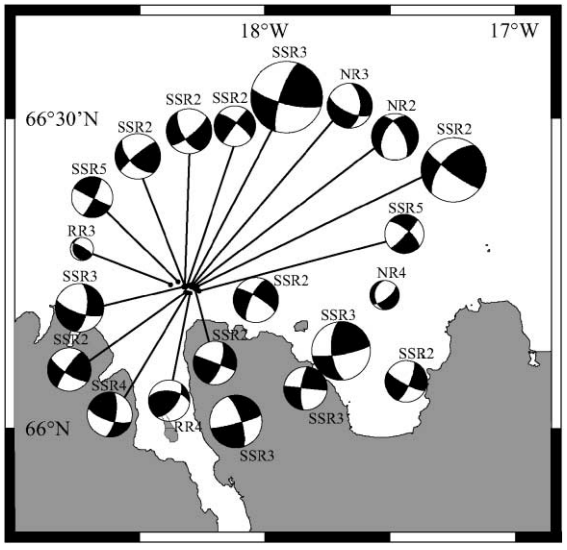

Fig. 7. Selection of focal mechanisms of earthquakes for the nine different determined regimes (SSR: strike-slip regime, NR: normal regime, RR: reverse regime). For all the regimes, excepted NR4 and RR3 regimes, only focal mechanisms of earthquakes with a magnitude bigger than M_L 2.5 are shown. For NR4 and RR3 regimes, only two focal mechanisms of earthquake are shown with respectively a magnitude of M_L 2.1 and M_L 1.6, respectively. The size of the balls is proportional to the magnitude of the earthquake.

a single stress regime is necessary to account for the data set. Considering such mechanical incompatibilities, the three mechanical groups used were separated in nine classes. These nine classes consist of four strike-slip states of stress (called SSR2, SSR3, SSR4 and SSR5), three extensive states of stress (NR2, NR3 and NR4) and two compressive states of stress (RR3 and RR4) (see Fig. 7).

The dominant states of stress (in terms of numbers of focal mechanisms) are of strike-slip type: SSR2 (31.4%) and SSR3 (33.2%) (Table 3). Normal-slip states of stress reveal a slight predominance of NR3 (8.2%) relative to NR2 (5.4%) and NR4 (4.8%). Reverse-slip states of stress display clear predominance of RR3 (9.5%) relatively to RR4 (1.8%).

4.3. From focal mechanisms to stress states

The main difference between the fault slip data collected in the field and the focal mechanisms of earthquakes based on earthquake records lies in the presence of two nodal planes in the second case. It is generally impossible, or very difficult, to decide which of these nodal planes is the active fault plane, which result in a major difficulty while carrying out the stress inversion, because most minimisation criteria depend on the choice of the nodal plane (Angelier, 1984).

Where the geological context is known, a simple solution of this problem consists in determining for each mechanism the nodal plane that best fits the geological structures. A second solution consists in selecting the nodal plane that best fits the stress tensor. Because this process tends to select the data according to the predicted result, and hence is somewhat circular, it cannot be regarded fully satisfactory. As a third solution, one of us (Angelier, 1998) developed a new method of inversion of focal mechanisms that is free of the uncertainty on the fault plane between the two nodal planes. The total data set (669 events) was processed using this new inversion method.

In this method, the misfit estimator (Rap in Table 4) ranges from −100% (largest misfit) to +100% (best fit). The negative values indicate a sense of shear opposed to that of slip. As a consequence, an estimator of 58% (the lowest value of Table 4) is a quite acceptable, and 80% (a common value in Table 4) indicates a severe demand for good fits. The average angle between the computed shear stress and the slip vector (Ang) is added to Table 4. This angle generally decreases as the demand for smaller misfits (higher estimators) increases. A value of about 20◦ (the largest average angle in Table 4) may seem relatively large; note, however, that for each focal mechanism this value is an average between the two angles that correspond to the two nodal planes.

4.4. Present-day stresses

Using the inversion method developed by Angelier (1998), the stress tensors have been determined for the nine groups separated above (Table 4). The inversion result for the NR2 group is shown in Fig. 8 as an example. For the strike-slip states of stress (SSR2, SSR3, SSR4 and SSR5), the minimum computed stress axes (σ_3) strikes N076°E, N056°E, N141°E and N002°E, respectively (Fig. 9). For the normal states of stress (NR2, NR3 and NR4), it strikes N092°E, N058°E and N122°E, respectively. The other states of stress (RR3 and RR4) are reverse in type and display computed N049°E and N138°E trends of compression (σ_1 axis).

In order to recognise the stress states that drive displacement on the HFF, a second inversion has been conducted giving to each earthquake a weight proportional to its magnitude. Concerning the strike-slip ruptures, which are the most frequent and correspond to the largest earthquakes, the new inversion yields similar stress orientation (Table 4). For the normal and reverse states of stress, differences were noticed (Table 4). The changes resemble a $\sigma_2-\sigma_3$ permutation for the reverse states of stress (e.g., the RR4 regimes) and a $\sigma_1-\sigma_2$ permutation for the normal states of stress (e.g., the NR4 regimes). Accordingly, low and high values of the Φ ratio where obtained in these two cases, respectively. Thus, after the weighted inversion, the strike-slip character of the stress states increased enough to be more important than the normal or reverse character, as compared with the initial inversion. This observation has important seismotectonic implications, namely that the largest earthquakes, regardless of the state of stress to witch they belong, are related to the transform motion. In other words, the large magnitude earthquakes reveal a regional stress field tightly related to the transform motion, whereas the low-magnitude earthquakes depend on the local stress fields.

Table 4
Results of the direct inversion of the focal mechanisms of earthquakes, without or with magnitude's weighting

	No weighting focal mechanisms									Magnitude's weighting focal mechanisms								
	σ_1		σ_2		σ_3		ϕ	Ang	Rap	σ_1		σ_2		σ_3		ϕ	Ang	Rap
	S	D	S	D	S	D				S	D	S	D	S	D			
SSR2	346	3	120	86	256	3	0.5	18	82	346	2	119	87	256	3	0.5	18	82
SSR3	146	8	319	82	56	1	0.5	16	85	146	7	316	83	56	1	0.5	17	84
SSR4	231	6	13	82	141	5	0.5	21	77	232	6	17	83	141	4	0.5	21	77
SSR5	272	1	14	85	182	5	0.5	19	78	271	2	19	85	181	5	0.5	18	79
NR2	344	72	184	17	92	6	0.6	13	88	356	33	199	55	93	11	0.7	15	64
NR3	158	69	327	21	58	4	0.6	15	84	151	30	317	59	58	6	0.6	20	64
NR4	356	79	213	9	122	6	0.6	12	88	24	35	228	53	122	12	0.8	16	63
RR3	49	8	316	20	159	68	0.4	15	80	48	13	299	54	147	33	0.3	20	62
RR4	138	6	47	8	266	80	0.4	17	81	137	11	31	54	234	33	0.2	20	58

The nine stress states are specified (SSR: strike-slip regime, NR: normal regime, RR: reverse regime). The strike (S) and dip (D) are given for each stress axis. See text for the definition of Φ, Ang and Rap and explanations about the weighting.

Considering the same $\sigma_1-\sigma_2$ permutation as for the geological data, the strike-slip and normal states of stress that display similar trends of extension can be grouped pairwise. We consequently associate SSR2 with NR2, SSR3 with NR3 and SSR4 with NR4. We thus obtain three main tectonic regimes (Fig. 9 and Table 4). The SSR2-NR2 regime reveals an ENE–WSW extension, SSR3–NR3 reveals NE–SW extension and SSR4–NR4 reveals NW–SE extension. Three states of stress cannot be accounted for by such $\sigma_1-\sigma_2$ permutation (RR3 indicating NE–SW compression, RR4 indicating NW–SE compression and SSR5 indicating N–S extension). However, invoking a $\sigma_1-\sigma_3$ permutation, RR3 and RR4 can be associated with SSR3–NR3 and SSR4–NR4, respectively. Furthermore, the SSR5 regime, which shows a computed N092°E trending σ_1 axis, can be associated with SSR2–NR2 that revealed E–W extension through the same type of permutation (Fig. 9).

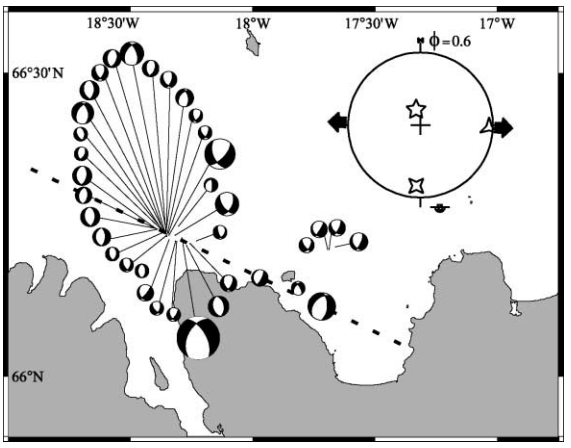

Fig. 8. Example of inversion of focal mechanisms of earthquakes applied to the NR2 data file. Diagram shows the inversion results (same symbols as in Fig. 5). The dotted line indicates the main trend of the HFF. See text for a definition of the Φ ratio.

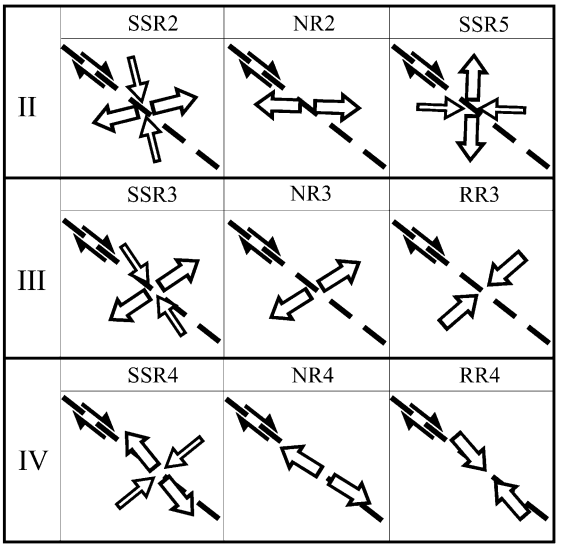

Fig. 9. Present-day stress states inferred from focal mechanisms of earthquakes (SSR, NR and RR: strike-slip, normal and reverse regimes, respectively). See text for detailed explanations concerning the grouping in three tectonic groups. Same symbols as in Fig. 6. North on the upward direction.

Based on such associations, we finally reconstructed three main groups of seismotectonic regimes (Fig. 9) labelled II, III and IV in order to underline their similarity with the groups defined based on geological data. The first two groups (groups II and III) respectively reflect ENE–WSW and NE–SW extensions, and respectively represent 43.2% and 39.5% of the data (Table 3). For group IV, it is difficult to decide whether extension or compression dominates because the contributions of the RR4 compressive state of stress on one hand and of the SSR4 and NR4 extensional states of stress on the other hand are comparable. This NW–SE extension or compression only represents 17.3% of the data (Table 3).

Some spatial and temporal correlations exist between the different states of stress of a same tectonic group. However, that they take place at the same time at the same place is not surprising; it simply brings confirmation of our regrouping. On the other hand, no significant spatial and temporal relationship could be found between the different tectonic groups, suggesting that they interact in a complex manner along the Húsavík–Flatey Fault.

5. Discussion and conclusion

5.1. Interpretation of the different trends of extension along the HFF

Three trends of extension did not change significantly between the Latest Cenozoic brittle deformation (Fig. 6 and Table 2) and the present-day seismicity (Fig. 9 and Table 4). These extension trends are ENE–WSW (groups II in Figs. 6 and 9), NE–SW (groups III in Figs. 6 and 9) and NW–SE (groups IV in Figs. 6 and 9).

However, 39.6% of the geological brittle data enabled us to define a tectonic group that we could not recognise in the inversion of the focal mechanisms, which strongly suggests that it does not exist at the present-day. These data belong to the S1–N1 regime with an average N103±8°E trend of extension, and to its opposite regime, the S6–N6 regime (with a N111±7°E trend of maximum horizontal stress). This direction of extension is almost the same as the direction of the plate relative motion at the TFZ, which is N106°E according to the NUVEL-1 model (DeMets et al., 1990; 1994). These regimes reflect an early stage of structural development prior to the development of the TFZ, during which the deformation was controlled by the oceanic rifting process. The relative chronology discussed before (see Section 3.4) supports this interpretation, because it indicates that the S1–N1 regime predates the other regimes. Strike-slip faults dominates among faulting associated with the S1–N1 regime and the S6–N6 opposite regime (Table 2), although one might expect a larger proportion of normal faulting during a rifting event. It has been shown, however, that strike-slip regimes commonly accompany the rifting process in Iceland (Bergerat et al., 1988, 1990; Passerini et al., 1997), so that in the regional context this large proportion can not be regarded surprising.

The other major extension trend, documented by both the brittle tectonic data (30.8%) and the focal mechanisms of earthquakes (39.5%), is ENE–WSW (groups II in Figs. 6 and 9). The WNW–ESE trending HFF is oblique relative to the N–S rift trends and to the E–W divergent plate motion. Extension is required in the transform zone, in order to compensate the created gap that would normally result from this obliquity (Bonatti, 1978; Gudmundsson et al., 1993; Gudmundsson, 1995). The major ENE–WSW transtension—combining extension and dextral shear—fulfils this geometrical requirement. Not surprisingly, strike-slip regimes prevail (Tables 2 and 3) in both the brittle tectonic data and the focal mechanisms of earthquakes.

A NE–SW extension, nearly perpendicular to the trend of the HFF, also occurs (groups III in Figs. 6 and 9). A similar extension had been noticed by several authors (Gudmundsson et al., 1993; Langbacka and Gudmundsson, 1995; Angelier et al., 2000; Bergerat et al., 2000). Normal faults associated with this NE–SW extension dominate among the geological data (Table 2), whereas most earthquakes reveal strike-slip faulting (Table 3): the present-day seismotectonic activity seems to be characterised by an increasing proportion of strike-slip mechanisms as compared with the long-term tectonic activity. However, this increasing proportion of strike-slip mechanisms can be a temporary phenomena amplified by the short time of recording considered herein. This is compatible with the anomalous size of the seismological data set (43%, considering the SSR3, NR3 and RR3 regimes) comparatively to the geological data set (15%, considering the S3–N3 regime).

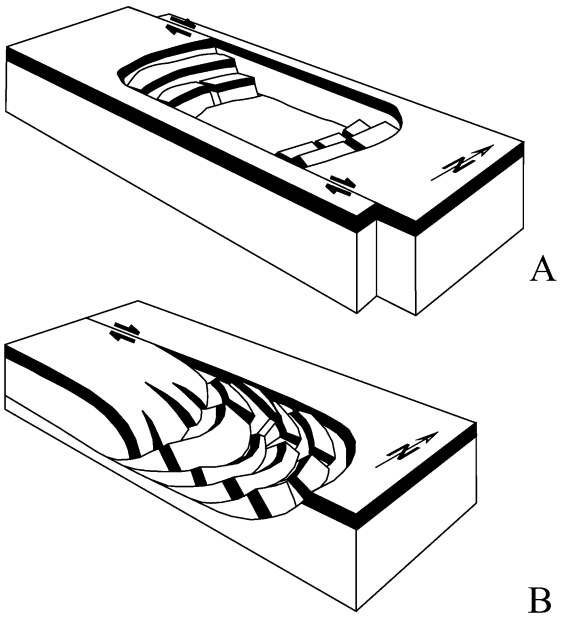

Fig. 10. The two proposed hypotheses for explaining the extension sub-parallel to the HFF. (A) Development of pull-apart structure. (B) Imbricate fan of normal faults (modified from Twiss and Moores, 1992).

A NW–SE extension (group IV in Figs. 6 and 9) is revealed by strike-slip faults and normal faults both for brittle data and focal mechanisms (Tables 2 and 4). However, the proportion of reverse-type focal mechanisms, corresponding to a NW–SE compression, is slightly more important than the strike-slip-type and normal-type focal mechanisms taken together (Table 4). In the other hand, no NW–SE compression could be identified with our brittle tectonic data, expect for a single paleostress tensor that was included in S3 because its Φ ratio was equal to 0. NE–SW trending structures, like dykes, normal faults or veins, have been identified by several authors (Saemundsson, 1974; Young et al., 1985; Fjäder et al., 1994; Langbacka and Gudmundsson, 1995). These NW–SE movements are sub-parallel to the average trend of the HFF. Movements along pull-apart or push-up structures could explain these NW–SE extensions or compressions (Fig. 10A). The "en échelon" structure of the HFF on land, with two pull-apart basins recognised on the Tjörnes Peninsula by Gudmundsson et al. (1993), support this hypothesis. These NW–SE movements can also be related to imbricate fans of normal or reverse faults at the termination of transform fault segments (Fig. 10B). Both hypothesis result from large-scale displacement along the HFF.

5.2. Seismotectonic behaviour of the HFF

According to our analysis of the geological data and the seismic data, the tectonic and seismotectonic behaviour of the HFF is characterised by a major dextral transtension and by two minor extensions, sub-parallel and sub-perpendicular to the transform fault. The two minor extensions are thought to correspond to a slip partitioning of the major dextral transtension in two minor regimes (Fig. 11). Similar slip partitioning in oblique context is a common phenomena in transform zones and has been described for the Dead Sea transform (Garfunkel, 1981), the Kane Fracture Zone (Garfunkel, 1986), the Vema Fracture Zone (Van Andel et al., 1971), the Romanche Fracture Zone (Bonatti, 1978) and the San Andreas and Sumatra Faults (Mount and Suppe, 1987; 1992). This dominant transtensional deformation is supported by the magnitude-weighted inversion of focal mechanisms, which shows that most large magnitude earthquakes are consistent with the regional stress field in relation with the transform motion, whereas the low-magnitude earthquakes depend on the local stress fields.

We also characterised an early stage of oceanic rifting process that predates the transform one (see Section 5.1). No chronological relationship for the three transform regimes (the dextral transtension, the

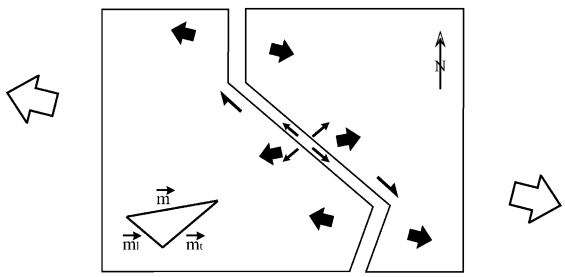

Fig. 11. Kinematic model of the HFF. The large white arrows show the direction of plate motion; the black arrows indicate the extensional direction (major phenomena are noticed by bigger arrows than for minor phenomena). The total displacement vector $\vec{m}$ at the HFF breaks up in a transversal displacement vector $\vec{m}_t$ and in a lateral displacement vector $\vec{m}_l$.

HFF-perpendicular and the HFF-parallel movements) was clearly established using brittle data (see Section 3.4). Moreover, during the 3-year period of focal mechanism recordings used in this study, the three transform regimes occurred, and without any clear spatial and temporal correlation (see Section 4.4). If correct, this observation implies that the three transform regimes do not occur as a definite succession of tectonic events, but rather as random local tectonic successions. Thus, for a given time span, one should not expect to find the same succession at different locations in the transform zone. This random local successions geographically distributed as moving patches within the deformed area explain why it is so difficult to establish a clear chronology of the tectonic regimes related to the transform motion. Furthermore, this interpretation is in good agreement with the concept of geometric accommodation in the transform zone.

The model proposed by Young et al. (1985) for the tectonic behaviour of the HFF was based on an interpretation of the observed deformations (tilted blocks and evolutions of the dyke trends) in terms of an unique tectonic process that implies a 110◦ clockwise rotation in an 11-km-wide dextral simple shear deformation zone. This differs from our model that combines strike-slip and extensional deformations and implies the existence of several stress states to explain the deformation. A small tectonic rotation is however conceivable in such an important shear zone, but our outcrop density, especially at the interior of the peninsula, does not allow defining an accurate spatial variation of the brittle deformation. On the other hand, Fjäder et al. (1994) considered that in addition to dextral shear, considerable extension has occurred across the HFF. However, the three extensions that they mentioned follow a chronological order that we were unable to determine. Based on the same data, but considering mainly the dyke orientations, Gudmundsson and Fjäder (1995) assumed that an extinct rift exists along the western boarder of the Flateyjarskagi Peninsula. They opined that tensile stresses perpendicular to this extinct ridge and to the transform fault gave rise to a stress field that explains the curved fabric and other structural elements on the Flateyjarskagi Peninsula (i.e., at a ridge-transform junction). It seems difficult to compare our reconstruction with this model, because the geological context considered is not the same.

Our study was carried out at two contrasting time scales. It allowed characterisation of the behaviour of the HFF involving a major dextral transtension that underwent slip partitioning in two other minor movements, sub-parallel and sub-perpendicular to the transform fault. In this respect, a rather stable picture of the tectonic–seismotectonic regimes that prevail in the transform zone emerges from our study. The necessity of extension in the transform zone appears to be a determining factor controlling the behaviour of the HFF.

Acknowledgements

Financial support was provided by the European Commission (contracts ENV4-CT97-0536 and EVR1-CT-1999-40002), the IFRTP (Arctic Program No. 316) and by the French–Icelandic scientific–cultural collaboration program (Iceland Ministry of Education and Culture and French Ministère des Affaires Etrangères).

We thank the Icelandic Meteorological Office, particularly Ragnar Stefánsson, director of the SIL program, for providing us the seismological data. Reviews by Jean-Pierre Burg, Agust Gudmundsson, and an anonymous reviewer improved the manuscript. We thank Jón Thorsteinsson for successful boat trips during the fieldwork and the French Embassy in Iceland for its help. (Figs. 1, 2, 7 and 8) were designed using the GMT software.

References

Anderson, E.M., 1942. The Dynamics of Faulting. Ed. Oliver and Boyd, Edinburgh.

Angelier, J., 1984. Tectonic analysis of fault slip data sets. Journal of Geophysical Research 89, 5835–5848.

Angelier, J., 1990. Inversion of field data in fault tectonics to obtain the regional stress—III. A new rapid direct inversion method by analytical means. Geophysical Journal International 103, 363–376.

Angelier, J., 1994. Paleostress analysis of small-scale brittle structures. In: Hancock, P. (Ed.), Continental Deformation. Pergamon, Tarrytown, NY, pp. 53–100.

Angelier, J., 1998. A new direct inversion of earthquakes focal mechanisms to reconstruct the stress tensor, European Geophysical Society. Annales Geophysicae 1, 115.

Angelier, J., Bergerat, F., 1983. Systèmes de contrainte et extension intracontinentale. Bulletin des Centres de Recherche Exploration–Production Elf-Aquitaine 7, 137–147.

Angelier, J., Mechler, P., 1977. Sur une méthode graphique de recherche des contraintes principales également utilisable en tectonique et en séismologie: la méthode des dièdres droits. Bulletin de la Societe Geologique de France 6, 1309–1318.

Angelier, J., Bergerat, F., Homberg, C., 2000. Variable coupling explains complex tectonic regimes near oceanic transform fault: Flateyjarskagi, Iceland. Terra Nova 12, 97–101.

Bergerat, F., Angelier, J., Villemin, T., 1988. Système de failles et états de contraintes sur une dorsale océanique émergée: l'Islande. Comptes Rendus de l'Academie des Sciences de Paris 307, 1397–1403.

Bergerat, F., Angelier, J., Villemin, T., 1990. Fault systems and stress patterns on emerged oceanic ridge: a case study in Iceland. Tectonophysics 179, 183–197.

Bergerat, F., Angelier, J., Homberg, C., 2000. Tectonic analysis of the Húsavík–Flatey Fault (northern Iceland) and mechanisms of an oceanic transform zone, the Tjörnes Fracture Zone. Tectonics 19, 1161–1177.

Björnsson, A., Johnsen, G., Sigurdsson, S., Thorbergsson, G., 1979. Rifting of the plate boundary in North Iceland 1975–1978. Journal of Geophysical Research 84, 3029–3038.

Bödvarsson, R., Rögnvaldsson, S.T., Jakobsdottir, S.S., Slunga, R., Stefansson, R., 1996. The SIL data acquisition and monitoring system. Seismological Research Letters 67, 35–46.

Bonatti, E., 1978. Vertical tectonism in oceanic fracture zones. Earth and Planetary Science Letters 37, 369–379.

DeMets, C.R., Gordon, R.G., Argus, D.F., Stein, S., 1990. Current plate motion. Geophysical Journal International 101, 425–478.

DeMets, C., Gordon, R.G., Argus, D.F., Stein, S., 1994. Effect of recent revisions to the geomagnetic reversal time scale on estimates of current plate motions. Geophysical Research Letters 21, 2191–2194.

Du, Y., Aydin, A., 1996. Elastic stress relaxation: a mechanism for opposite sense of secondary faulting with respect to a major fault. Tectonophysics 257, 175–188.

Einarsson, P., Björnsson, S., 1979. Earthquakes in Iceland. Jökull 29, 37–43.

Fjäder, K., Gudmundsson, A., Forslund, T., 1994. Dikes, minor faults and mineral veins associated with a transform fault in North Iceland. Journal of Structural Geology 16, 109–119.

Foulger, G.R., Jahn, C.H., Seeber, G., Voesken, C., Hofton, M.A., Hodgkinson, K.M., Julian, B.R., Heki, K., 1992. Stress Diffusion in NE Iceland Detected Using GPS, and the 1992 Resurvey, AGU 1992 Fall Meeting. EOS, 118.

Garfunkel, Z., 1981. Internal structure of the Dead Sea leaky transform (rift) in relation to plate kinematics. Tectonophysics 80, 81–108.

Garfunkel, Z., 1986. Review of oceanic transform activity and development. Journal of Geological Society of London 143, 775–784.

Gudmundsson, A., 1995. Stress fields associated with oceanic transform faults. Earth and Planetary Science Letters 136, 603–614.

Gudmundsson, A., 2000. Dynamics of volcanic systems in Iceland: example of tectonism and volcanism at juxtaposed hot spot and mid-ocean ridge systems. Annual Review of Earth and Planetary Sciences 28, 107–140.

Gudmundsson, A., Fjäder, K., 1995. Dikes, minor faults and mineral veins associated with a transform fault in North Iceland: reply. Journal of Structural Geology 17, 1633–1636.

Gudmundsson, A., Brynjolfsson, S., Jonsson, M.T., 1993. Structural analysis of a transform fault–rift zone junction in north Iceland. Tectonophysics 220, 205–221.

Gudmundsson, A., Berg, S.S., Lyslo, K.B., Skurtveit, E., 2001. Fracture networks and fluid transport in active fault zones. Journal of Structural Geology 23, 343–353.

Helgason, J., 1984. Frequent shifts of the volcanic zone in Iceland. Geology 12, 212–216.

Helgason, J., 1985. Shifts of the plate boundary in Iceland: some aspects of tertiary volcanism. Journal of Geophysical Research 90, 10084–10092.

Jancin, M., Young, K.D., Voight, B., 1985. Stratigraphy and K/Ar ages across the west flank of the Northeast Iceland axial rift zone, in relation to the 7 Ma volcano-tectonic reorganisation of Iceland. Journal of Geophysical Research 90, 9961–9985.

Jancin, M., Young, K.D., Voight, B., Orkan, N.I., 1995. Dikes, minor faults and mineral veins associated with a transform fault in North Iceland: discussion. Journal of Structural Geology 17, 1627–1631.

Langbacka, B.O., Gudmundsson, A., 1995. Extensional tectonics in the vicinity of a transform fault in north Iceland. Tectonics 14, 294–306.

McKenzie, D.P., 1969. The relation between fault plane solutions for earthquakes and the directions of the principal stresses. Bulletin of the Seismological Society of America 59, 591–601.

McMaster, R.L., Schilling, J.-G.E., Pinet, P.R., 1977. Plate boundary within Tjörnes Fracture Zone on Northern Iceland's insular margin. Nature 269, 663–668.

Möller, D., Ritter, B., 1980. Geodetic measurements and horizontal crustal movements in the rift zone of NE-Iceland. Journal of Geophysics 4, 110–119.

Mount, V.S., Suppe, J., 1987. State of stress near the San Andreas Fault: implications for wrench tectonics. Geology 15, 1143–1146.

Mount, V.S., Suppe, J., 1992. Present-day stress orientations adjacent to active strike slip faults: California and Sumatra. Journal of Geophysical Research 97, 11995–12013.

Passerini, P., Marcucci, M., Sguazzoni, G., Pecchioni, E., 1997. Longitudinal strike slip faults in oceanic rifting: a mesostructural study from western to southeastern Iceland. Tectonophysics 269, 65–89.

Rögnvaldsson, S.T., Slunga, R., 1993. Routine fault plane solutions for local networks: a test with synthetic data. Bulletin of the Seismological Society of America 83, 1232–1247.

Rögnvaldsson, S.T., Gudmundsson, A., Slunga, R., 1998. Seismotectonic analysis of the Tjörnes Fracture Zone, an active transform fault in north Iceland. Journal of Geophysical Research 103, 30117–30129.

Saemundsson, K., 1974. Evolution of the axial rifting zone in northern Iceland and the Tjörnes fracture zone. Geological Society of America Bulletin 85, 495–504.

Slunga, R., 1981. Earthquake source mechanism determination by use of body wave amplitudes — an application to Swedish earthquakes. Bulletin of the Seismological Society of America 71, 25–35.

Stefansson, R., Bödvarsson, R., Slunga, R., Einarsson, P., Jakobsdottir, S., Bungum, H., Gregersen, S., Haskov, J., Hjelme, J., Korhonen, H., 1993. Earthquake prediction in the South Iceland Seismic Zone and the SIL project. Bulletin of the Seismological Society of America 83, 696–716.

Tryggvason, E., 1973. Seismicity, earthquake swarms and plate boundaries in the Iceland region. Bulletin of the Seismological Society of America 63, 1327–1348.

Twiss, R.J., Moores, E.M., 1992. Structural Geology. Ed. W.H. Freeman, New York, 532 pp.

Van Andel, T.H., Von Herzen, R.P., Phillips, J.D., 1971. The Vema fracture zone and the tectonics of transverse shear zone in oceanic crustal plates. Marine Geophysical Researches 1, 261–283.

Ward, P.L., 1971. New interpretation of the geology of Iceland. Geological Society of America Bulletin 82, 2991–3012.

Wendt, K., Möller, D., Ritter, B., 1985. Geodetic measurements of surface deformations during the present rifting episode in NE Iceland. Journal of Geophysical Research 90, 10163–10172.

Young, K.D., Jancin, B., Orkan, N.I., 1985. Transform deformation of tertiary rocks along the Tjörnes Fracture Zone, North Central Iceland. Journal of Geophysical Research 90, 9986–10010.